Interpretation of the high spin states in ^{161}Lu: A paired and unpaired study

Hai-Liang Ma,[1,2,*] B. Gillis Carlsson,[1] Ingemar Ragnarsson,[1,†] and Hans Ryde[1]
[1]*Division of Mathematical Physics, LTH, Lund University, P.O. Box 118, SE-221 00 Lund, Sweden*
[2]*China Institute of Atomic Energy, P.O. Box 275-10, Beijing 102413, People's Republic of China*
(Received 22 May 2014; published 23 July 2014)

A paired cranked Nilsson-Strutinsky-Bogoliubov (CNSB) model is presented, which employs the same method to calculate the liquid-drop energy and moment of inertia as the unpaired cranked Nilsson-Strutinsky (CNS) model. In the CNSB model, the energy minimization is carried out in the mesh of pairing gaps Δ and Fermi levels λ as well as deformation parameters. The high spin states in ^{161}Lu are then investigated with the CNSB and CNS models. The terminating structure shows a striking similarity with these two models. Combining the CNSB and CNS models, a complete understanding of high spin structures, including the normal deformed (ND) and triaxial strongly deformed (TSD) bands and observed side bands in ^{161}Lu, is achieved. It appears that the only important paired crossings are the first $i_{13/2}$ neutron crossing and the first $h_{11/2}$ proton crossing. For the description of the unpaired high spin crossings, it is important to be able to distinguish between the pseudospin partners in the proton $\mathcal{N} = 4$ shell, $(d_{5/2},g_{7/2})$ and $(d_{3/2},s_{1/2})$. The yrast bands are predicted to terminate, which explains the structure of a TSD-like band X2. A band crossing at $I \approx 36.5$ for the TSD band in ^{161}Lu, unique within the chain of even-N Lu isotopes, is well described by the CNSB model.

DOI: 10.1103/PhysRevC.90.014316 PACS number(s): 21.10.Re, 21.60.Ev, 23.20.Lv, 27.70.+q

I. INTRODUCTION

As a result of pairing interaction the shapes of rotational structures in the low spin region of even-Z and even-N nuclei are markedly influenced. The well-known backbending phenomenon is caused by pairing being broken through the alignment of two quasiparticles. As the nucleus rotates even faster, more quasiparticles can be aligned such that the nuclear superfluidity can be destroyed at some critical frequency [1,2] and eventually lead to the pairing collapse. The static pairing effect is negligible and only the dynamic pairing will have effects beyond this frequency [3].

In the nuclear structure studies, the pairing correlation is usually treated by the Bardeen-Cooper-Schrieffer (BCS) or Hartree-Fock-Bogoliubov (HFB) approximations [4]. However, such approximations without particle number projection suffer a sharp phase transition from a superfluid to an unpaired phase [5,6] and eventually lead to the pairing collapse at some critical frequency [2,3]. The number-projected HFB on the other hand shows a smooth transition, in complete agreement with the exact solutions [6]. In addition to the static pairing which can be reproduced by the BCS approach, the dynamic pairing is implicitly included in the number-projected HFB approach, which gives the dominating contribution at high spins [3].

The cranked Nilsson-Strutinsky-Bogoliubov (CNSB) model which adopts the particle-number projection (PNP) and treats the pairing parameters self-consistently was introduced in Ref. [7]. By varying the total energy with respect to the pairing gaps and the Fermi levels, the present CNSB model is equivalent to the solution of the number-projected HFB where the pairing gap is determined by the self-consistent iterations [6,8,9]. Although much more computational power is needed for a mesh calculation in the CNSB model, it prevents the reiteration of pairing gap as well as recalculation of the density matrix and the paring tensor in the self-consistent number-projected HFB approach, which also might bring unphysical crossings when removing the virtual interactions. The variation of the Fermi level adopted in the CNSB model is also extremely important for terminating or near-terminating states. With multiple quasiparticles aligned, the optimal Fermi level that gives the correct particle number and the lowest total energy can deviate markedly from the one determined at $\omega = 0$. In this paper, the macroscopic energy and moment of inertia in the CNSB model are taken the same as the unpaired cranked Nilsson-Strutinsky (CNS) model [10]. Many analyses of high spin data throughout almost the entire nuclear chart are based on the latter formalism. The virtual crossings are removed both in the CNS and CNSB model. By comparing the paired and unpaired calculation results, the pairing effect in the entire spin region can be studied.

Abundant rotational structures have been established in the Lu isotopes [11–15] which roused much attention both from experiment and theory, especially that the wobbling motion is expected. In ^{161}Lu, in addition to the triaxial strongly deformed (TSD) bands, the second back-bending, the termination of the normal deformed (ND) bands, and the side bands are also of interest. The side band X2 is of particular interest. Its aligned angular momentum is similar to that of the TSD bands but it is much lower in energy. Indeed, it was assigned as a terminating band in Ref. [16], an interpretation that might shed light on the assignment of similar bands observed in this mass region, such as the recently observed TSD-like bands in ^{164}Hf [17]. The theoretical information on the termination of the yrast bands and properties of the TSD bands could be useful for future experimental studies. Moreover, the rich physics also makes ^{161}Lu a good testing ground for the models.

*hailiang.ma@matfys.lth.se
†Ingemar.Ragnarsson@matfys.lth.se

In this paper, we carried out paired CNSB and unpaired CNS calculations to investigate the rotational structures in ^{161}Lu. The description of the CNSB model is given in Sec. II. A detailed interpretation of the yrast, side, and TSD bands will be shown in Sec. III. The effect of pairing correlation in the entire spin region and comparison between the results of paired and unpaired calculations are also discussed. The paper is summarized in Sec. IV.

II. CRANKED NILSSON-STRUTINSKY-BOGOLIUBOV MODEL

The general features of the cranked Hartree-Fock-Bogoliubov model are discussed, for example, in [4] and the version used in this work is discussed in [7,18]. The Hamiltonian is taken as

$$H = \sum_{q=p,n} \left[h_q^{\mathrm{MO}}(\bar{\varepsilon}) - G_q P_q^{\dagger} P_q\right], \tag{1}$$

where h_q^{MO} denotes the modified oscillator potential and the label q runs over protons(p) and neutrons(n). $\bar{\varepsilon}$ is a shorthand notation for the quadrupole (ε_2,γ) and hexadecapole ε_4 deformation parameters. $P^{\dagger}$ and P represent the pair creation and annihilation operators, respectively. This leads to the HFB single-particle cranking Hamiltonian [4]:

$$H_{\omega} = \sum_{q=p,n} \left[h_q^{\mathrm{MO}}(\bar{\varepsilon}) - \omega_x (j_x)_q - \Delta_q (P_q^{\dagger} + P_q) - \lambda_q \hat{N}_q\right]. \tag{2}$$

In this expression, $-\omega_x j_x$ denotes the cranking term, Δ the pairing gap, λ the Fermi level, and $\hat{N}$ is the particle number operator. The solution of the cranking Hamiltonian gives rise to quasiparticle energies that depend on the cranking frequency. The quasiparticles are connected diabatically between the ω mesh points removing virtual crossings [7,18] and a specific quasiparticle excitation defines a configuration. All such configurations that are low in energy are constructed and for each of them we obtain wave functions Ψ dependent on Δ, λ, ω, ε_2, γ, and ε_4.

With the HFB approach these wave functions do not have fixed particle numbers and to correct for this we calculate the particle-number projected energy:

$$E_p(\omega,\Delta_p,\lambda_p,\bar{\varepsilon}) = \frac{\langle\Psi|H P^Z|\Psi\rangle}{\langle\Psi|P^Z|\Psi\rangle}, \tag{3}$$

where P^Z denotes the particle-number projection operator for protons. The energy for neutrons can be obtained analogously, so that the total unrenormalized energy now reads

$$E = E_p(\omega,\Delta_p,\lambda_p,\bar{\varepsilon}) + E_n(\omega,\Delta_n,\lambda_n,\bar{\varepsilon}). \tag{4}$$

We employ the macroscopic-microscopic approach that was extensively used in the calculation of nuclear masses and high spin spectra [10,19]. In this approach the total energy is obtained through the Strutinsky method [18,20] and interpolation is used to obtain values for fixed $I \approx I_x$. In the Strutinsky method the smoothed energy $\tilde{E}$ is constructed and subtracted from the unrenormalized total energy E to give the fluctuating part of the energy δE. The renormalized total nuclear energy is then obtained by summing the rotating liquid drop energy E_{RLD} and δE and minimizing with respect to the deformation and pairing parameters:

$$E_{\mathrm{tot}}(Z,N,I) = \min_{\bar{\varepsilon}\lambda_p\lambda_n\Delta_p\Delta_n} [E_{\mathrm{RLD}}(Z,N,I,\bar{\varepsilon}) + \delta E(Z,N,I,\bar{\varepsilon},\lambda_p,\lambda_n,\Delta_p,\Delta_n)]. \tag{5}$$

Note that for the pairing energy, the Strutinsky smoothing procedure is not performed. Because the pairing term is not in the macroscopic energy, the same E_{RLD} can be used as in the unpaired case. This has the advantage of making a direct comparison of the results of paired and unpaired calculations possible. The minimization in Eq. (5) is done for each configuration and then the 16 yrast lines corresponding to preserved signatures and parities of protons and neutrons are obtained by taking the lowest states within the groups for each angular momentum I.

In this work we calculate the macroscopic rotating liquid drop energy, using the Lublin-Strasbourg drop model (LSD) [21],

$$E_{\mathrm{RLD}}(Z,N,I,\bar{\varepsilon}) = E_{\mathrm{LD}}(Z,N,\bar{\varepsilon}) + \frac{\hbar^2 I(I+1)}{2\mathcal{J}_{\mathrm{rig.}}}, \tag{6}$$

where E_{LD} is the static liquid drop energy and $\mathcal{J}_{\mathrm{rig}}(Z,N,\bar{\varepsilon})$ is the rigid-body moment of inertia. The same correction as in Ref. [22] is used to remove the average pairing and zero-point energy that are generally obtained when fitting the liquid-drop expression to nuclear masses. The rigid-body moment of inertia is calculated with the radius parameter $r_0 = 1.16$ fm and the surface diffuseness parameter $a = 0.6$ fm [22].

Compared to unpaired calculations, the complexity caused by doubling the single-particle levels and mixing the particle-hole components in the pairing formalism makes it more difficult to describe rotating nuclei. But reaching the high spin regime where several quasiparticles are aligned, the pairing effect often plays a minor role and unpaired calculations can be used to characterize the rotational structures. In this case the unpaired CNS model [10,22] is often used as it enables accurate tracing of the configurations using the number of particles in different "deformed" j shells as approximate quantum numbers. Transparent interpretations of terminating states have been achieved using this model throughout the periodic table. In the CNS model, the virtual crossings are also removed. However, there is a vital difference between the unpaired and the paired calculations of the total energy. In the paired CNSB model, the quantities to be calculated are not only dependent on the quasiparticle Routhians, which are smooth after removing the virtual interaction, but also on the particle-hole component of the orbitals. This sometimes causes problems because the amplitude of a projected state may become too small as a function of the frequency. This problem does not exist in the unpaired calculations because the shell correction energy is dependent only on the single-particle Routhians. In this paper, the unpaired CNS model [22] is also used to investigate the terminating states in ^{161}Lu. Because the macroscopic models are the same for the unpaired CNS and paired CNSB models, a direct comparison is possible at high spins and enables the study of the pairing effects for terminating states. We have checked carefully that the

calculations with the CNS code are consistent with the CNSB code, if the pairing is turned off.

III. RESULTS AND DISCUSSION

The $A = 150$ parameters [10,23] are used in both paired and unpaired calculations. This set of parameters is tuned to describe the band termination phenomena in $A \sim 150$ nuclei. In the CNSB calculations, the pairing strength G is taken from Ref. [18]. Because the particle-number projection is employed, the pairing strength is reduced by a factor of 0.95, as suggested in Ref. [23]. In the paired calculations, the Δ mesh is set as $(\Delta_{\min}, \Delta_{\max}, d\Delta) = (0.3, 1.5, 0.15)$ MeV. The λ mesh contains nine values centered around the BCS value at $\omega = 0$ with a spacing of $d\lambda = 0.3$ MeV and different values are used for each deformation. Considering that the energy depends weakly on λ, no interpolation is implemented in the (Δ, λ) mesh to avoid fictive minima [7]. After minimizing the total energies with respect to deformation, the energies and deformations at specific spin values can be obtained.

Although it is generally accepted that the pairing correlations become weak at high spins, the information is limited on how much the rotational behavior is affected, when approaching the terminating states. A first such kind of comparison will be delivered in Sec. III A. After we discuss the yrast bands of ^{161}Lu in Sec. III C, we focus on the interpretation of several side bands in Sec. III D and their relations to the yrast bands. The properties of the TSD bands are discussed in Sec. III E.

A. Comparison between paired and unpaired calculations approaching the band termination

Usually the unpaired models are employed in the band terminating region, for example, see Ref. [10], and references therein. By varying the total energy with respect to the pairing gaps and Fermi levels, the present CNSB code is capable of reaching the terminating states with the dynamic pairing correlation included, i.e., it becomes possible to draw smooth energy surfaces in the full (ε_2, γ) plane. Because parity π and signature α are conserved quantum numbers with the present Hamiltonian, in total 16 combinations designated with $(\pi_p, \alpha_p)(\pi_n, \alpha_n)$ can be formed. The comparison of paired and unpaired results of these 16 yrast bands in their full spin range are shown in Figs. 1 and 2 for the positive and negative parities, respectively. In the figures the reference energies of a rotating liquid drop are subtracted. From Figs. 1 and 2 it is interesting to note that the relative energies with and without pairing appear similar in the $I = 40$–50 spin range but the moments of inertia become rather different already in the $I = 30$–40 spin range. In a few cases, the order in energy of the bands changes in the lower spin range. For example, the $(-, \pm 1/2)(-, 1)$ bands are relatively lower in energy in the CNSB model than in the CNS model. For terminating states with $I \gtrsim 50$ and beyond, however, the similarity of the spectral structure between the paired and unpaired results are striking.

The energy differences between the unpaired and paired results, which can be seen as the pairing correction energies, are displayed in Figs. 1(c) and 2(c). It is seen that the pairing

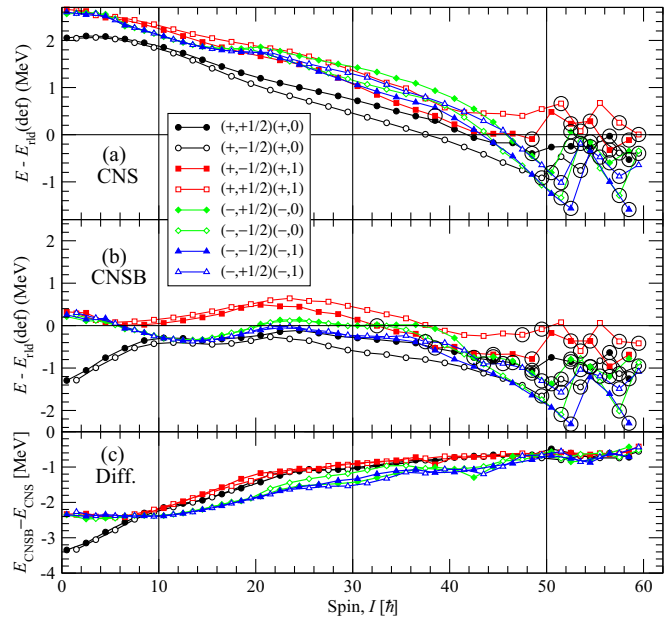

FIG. 1. (Color online) Unpaired (a) and paired (b) calculation results and their differences (c) in ^{161}Lu for the positive parity configurations. The aligned states at $\gamma = 60^\circ$ are indicated by large open circles.

correction energies for the configurations in ^{161}Lu follow the same trend for the different configurations. Thus if a smooth function is fitted to the curves in Figs. 1(c) and 2(c), the values for the different configurations would in general come within ± 0.3 MeV of this smooth function. This suggests that the absolute energy of the different bands could to a good approximation be described by the unpaired energy corrected with a schematic pairing energy.

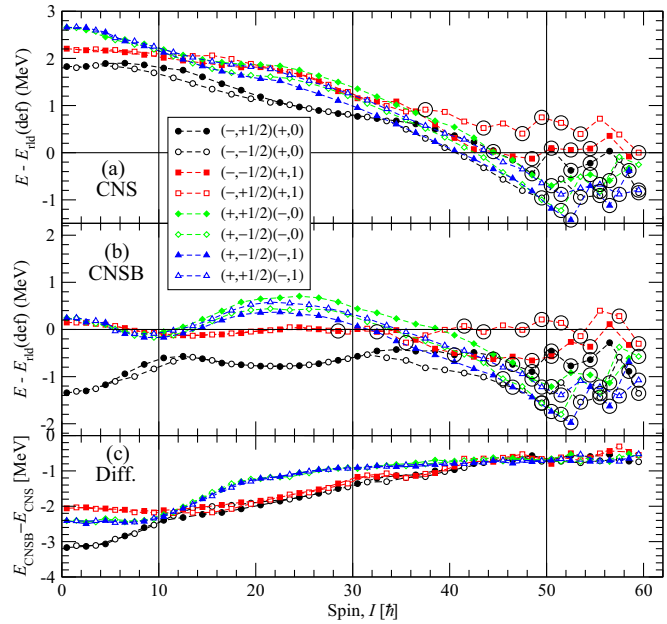

FIG. 2. (Color online) Same as previous figure but for the negative parity configurations.

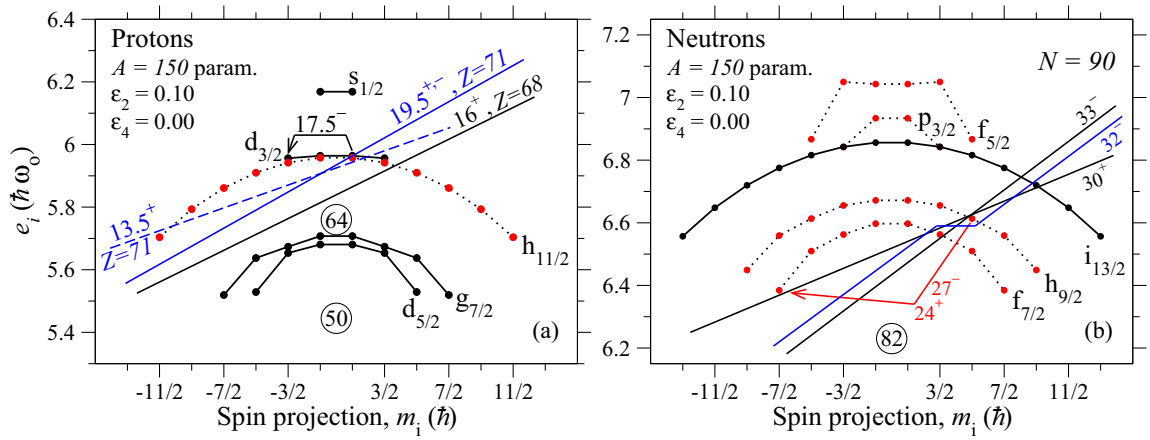

FIG. 3. (Color online) Single-particle energies e_i vs aligned spin m_i for protons (a) and neutrons (b) at $(\varepsilon_2,\gamma) = (0.1,60^\circ)$. Tilted Fermi surfaces for $Z = 71$ and 68, and $N = 90$ are drawn for the low-energy terminating spin states. For $Z = 71$ a proton spin state $I_p = 19.5$ with positive or negative parity is formed dependent on if the occupied $m_i = 1/2$ orbital belongs to the $h_{11/2}$ or $d_{3/2}$ subshell. It is shown by an arrow how the deexcitation from $m_i = 1/2$ to $m_i = -3/2$ in the proton $h_{11/2}$ and $d_{3/2}$ shells leads to proton spin $I_p = 17.5^{\pm}$ for $Z = 71$ and from $m_i = 5/2$ to $m_i = -7/2$ in the neutron $h_{9/2}f_{7/2}$ shells leads to neutron spins $I_n = 27^-$ and 24^+ (starting from the $I_n = 33^-$ and 30^+ states). Similarly, starting from the proton 19.5^+ state, a deexcitation in the $h_{11/2}$ orbitals, $m_i = 1/2 \rightarrow -11/2$ leads to an $I_p = 13.5^+$ state corresponding to the tilted Fermi surface drawn by a dashed line.

On the other hand, when it comes to the detailed variation of the total energy as a function of spin, it is essential to include the details of the pairing energy. Especially, paired crossings should show up as discontinuities in the differences in Figs. 1(c) and 2(c). There are essentially two such discontinuities, namely for $I \approx 10$ and $I \approx 20$, respectively, corresponding to the $i_{13/2}$ quasineutron crossing and the $h_{11/2}$ quasiproton crossing. The fact that there are no more significant discontinuities in these differences for ^{161}Lu suggest that calculated crossings at higher spin values are similar in the CNS and the CNSB formalism. In turn, this indicates that they can be understood as caused by crossings between unpaired single-particle Routhians.

B. The structure of terminating states

In Figs. 1 and 2 one notes that the calculated yrast states for spin values $I > 50$ are generally noncollective and associated with terminating bands. Except for Ref. [16] terminating states have not been discussed for ^{161}Lu and no experimental evidence for terminating bands have been reported. On the other hand, ^{158}Er with the same number of neutrons as ^{161}Lu and three protons less is a key nucleus for terminating bands [10,23,24]. Indeed, as illustrated in Fig. 3, comparisons with ^{158}Er gives an easy understanding of the terminating bands which are predicted in the yrast region of ^{161}Lu. In ^{158}Er, three bands are observed to low-energy terminations for spin values just below $I = 50$. Their configurations are illustrated in sloping Fermi surface diagrams in Fig. 3; i.e., the $I^\pi = 16^+$ proton $(h_{11/2})^4$ state is combined with the $N = 90$ $I^\pi = 30^+$, 32^-, and 33^- neutron states. These same neutron states give rise to six low-energy terminations in ^{161}Lu when they are combined with the two $I^\pi = 19.5^\pm$ states for $Z = 71$ as also illustrated in Fig. 3. Indeed, the bands in ^{161}Lu are quite interesting because the calculations indicate that they can be followed down to much lower spin values than the bands in ^{158}Er. The latter can only be followed a few transitions below the terminating state before they become nonyrast.

The bands in ^{161}Lu are calculated as yrast in a larger spin range because the Fermi level is higher for $Z = 71$ than for $Z = 68$. This means that it will be energetically more expensive for $Z = 71$ than for $Z = 68$ to create configurations with holes in the orbitals below the $Z = 64$ gap, i.e., the configurations which build the more collective low-energy configurations in the $I = 40$–50 spin range. On the other hand, the three extra protons for $Z = 71$ compared with $Z = 68$ do only contribute with a small angular momentum, $3.5\hbar$, which should disfavor terminations [10], but this fact appears to be of minor importance. The conclusion is then that ^{161}Lu should be an excellent playground to study terminations. However, terminations have not been identified in ^{161}Lu up to now, probably because they occur at such high spin values but also because experiments on ^{161}Lu have rather concentrated on TSD bands and possible wobbling excitations. Indeed, the present calculations show that the X2 band, which was suggested to be of the TSD type in Ref. [14], should instead be assigned to the terminating configuration which is calculated lowest in energy (see below).

It is also interesting to notice that the paired calculation predicts more aligned states compared with the unpaired calculation. Let us consider the $(+,-1/2)(-,1)$ and $(+,-1/2)(+,0)$ configurations whose terminating states are illustrated in Fig. 3, i.e., the 19.5^+ proton state is combined with the 33^- and 30^+ neutron states. Selected potential energy surfaces (PESs) of the $(+,-1/2)(-,1)$ configuration are shown in Fig. 4, while the energy of both configurations are shown relative to the rotating liquid drop energy in Fig. 5. In Fig. 3 it is then also shown how lower-spin noncollective configurations are formed if the spin vector of one of the valence particles points in the opposite direction. It is thus illustrated how six

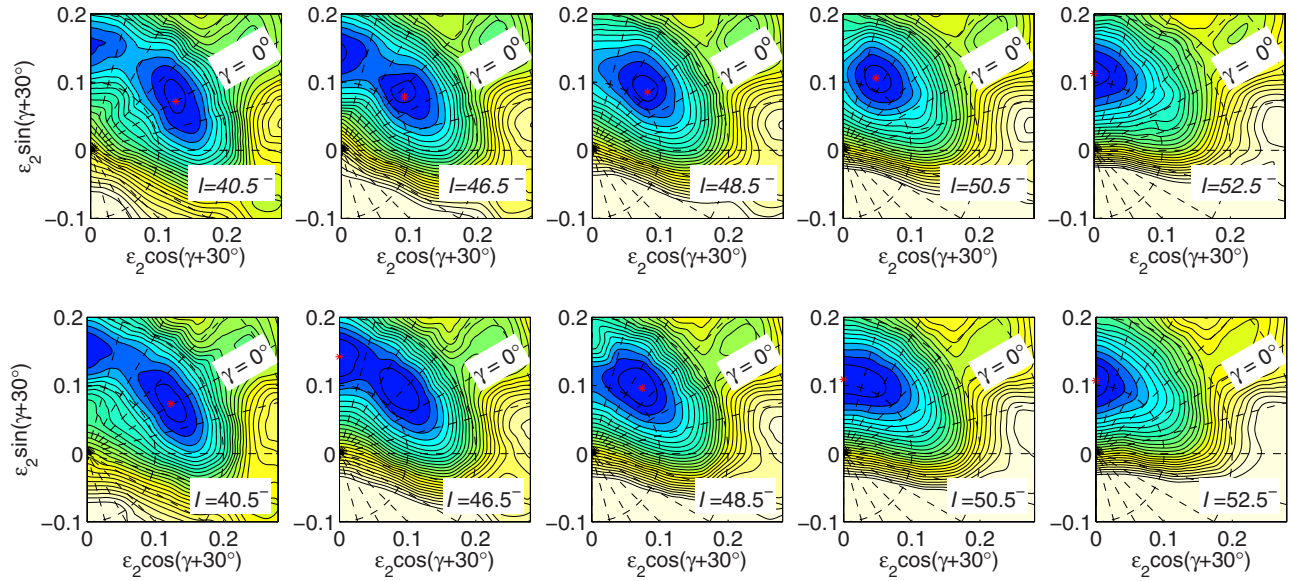

FIG. 4. (Color online) Calculated PESs for the configuration $(+,-1/2)(-,1)$ with the CNS (top) and CNSB (bottom) models. The global minima are marked by stars. The energy interval of contour lines is 0.2 MeV.

spin units are lost either by moving a neutron from $m_i = 5/2$ to $m_i = -7/2$ in the $\nu(h_{9/2}f_{7/2})$ orbitals or from $m_i = 1/2$ to $m_i = -11/2$ in the $\pi(h_{11/2})$ orbitals. The figure suggests that also these two states with one spin vector antialigned should be competitive in energy, because it is easy to see they

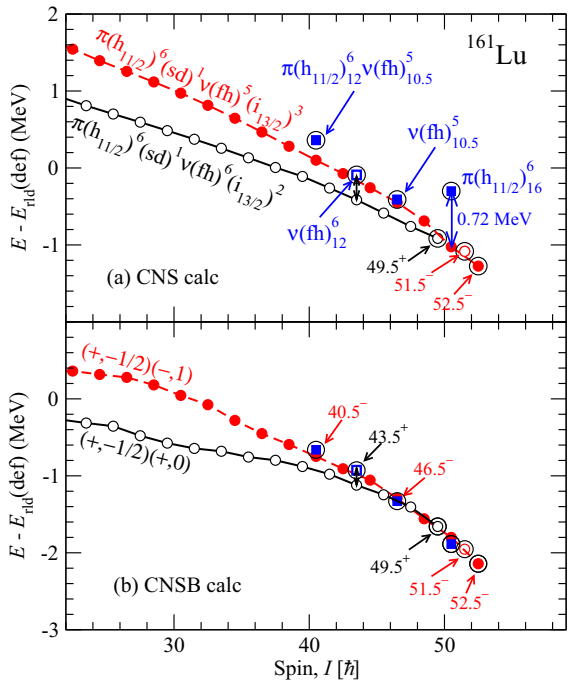

FIG. 5. (Color online) The collective and noncollective states in the CNS (a) and CNSB (b) calculations for the $(+,-1/2)(+,0)$ and $(+,-1/2)(-,1)$ configurations. Aligned states at $\gamma = 60^\circ$ are encircled. The full configuration for the two bands are specified relative to a ^{146}Gd core in panel (a). For nonfully aligned particles in the valence space, the spin content is specified by subscript.

can be formed from straight line or almost-straight-line Fermi surfaces. Thus, if one of these deexcitations is performed, aligned states six spin units below the terminating state are formed while an aligned state six spin units further down are formed with both deexcitations. In the potential energy surfaces, these aligned states show up as minima at $\gamma = 60^\circ$ which compete with a minimum at $\gamma < 60^\circ$ corresponding to the band which continues smoothly to the $I_{\max} = 52.5$ state. One may note that the corresponding neutron excitation in ^{158}Er leads to noncollective states at $I = 43^-$ and 40^+ which are clearly lower in energy than the smooth bands which terminate at $I = 49^-$ and 46^+, respectively [24]. In ^{161}Lu, the two minima for $I = 46.5^-$ and $I = 40.5^-$ are at similar energies. Looking at details, it turns out that for $I = 46.5^-$, the aligned state is lower in the CNSB calculation but not in the CNS calculation while it is slightly higher in energy in both approaches for $I = 40.5^-$.

It should be evident from Fig. 3 that aligned states and more collective states should compete also in some of the other terminating configurations. This is illustrated in Fig. 5 for the $I = 43.5^+$ state of the band terminating at $I = 49.5^+$. In this case, the aligned 43.5^+ state is higher in energy than the collective 43.5^+ state in both paired and unpaired calculations, but with the same tendency as noted above that pairing favors the aligned state. The fact that pairing lowers some aligned states can be understood from the observation that the lowered states are those where the particles in the valence space, i.e., in open shells, are not fully aligned. For such states there are still some nonaligned pairs remaining that can contribute to the correlation energy.

While most energy surfaces in Fig. 4 are similar in the CNS and CNSB calculations, the $I = 50.5$ state is an exception. In this case, the lowest energy corresponds to an aligned state when pairing is included, while the aligned state is ~0.7 MeV above the collective minimum in the unpaired case as seen more clearly in Fig. 5. The configuration of

this $I = 50.5$ state is illustrated in Fig. 3. Relative to the terminating $I = 52.5$ state, one proton is moved from the $m_i = 1/2$ to the $m_i = -3/2$ state. As these two single-particle states have a similar energy, the aligned $I = 50.5$ state will have a similar energy as the terminating $I = 52.5$ state in the unpaired case. Consequently, with the reference subtracted, it will come at a considerably higher energy as seen in Fig. 5. Then, however, the pairing energy is relatively large for the aligned $I = 50.5$. This can be understood from the fact that in this case, there are three orbitals close to the Fermi surface where both the spin projections m and $-m$ are either filled ($h_{11/2,\pm 3/2}$) or empty ($h_{11/2,\pm 1/2}, d_{3/2,\pm 1/2}$). These orbitals with strongly mixed particle-hole components can thus contribute to a relatively large pairing energy. In the simple case of BCS pairing with blocking, we have increased the pairing constant so that a superfluid solution is found and then verified that this deexcitation loosing two spin units gives rise to a considerably larger increase of the pairing energy than the other deexcitations illustrated in Fig. 3 loosing six spin units. The case illustrated in Figs. 4 and 5 corresponds to the aligned 19.5^+ proton state in Fig. 3, but the same arguments can be applied to the aligned 19.5^- state instead when the proton is again moved from $m_i = 1/2$ to the $m_i = 3/2$, but in this case within the orbitals of $d_{3/2}$ character. The conclusion is thus, that in general, the relative energy of aligned and nonaligned states in the terminating region is rather similar with and without pairing but with some tendency that pairing favors the aligned states. In specific cases, however, pairing can be more important giving a larger contribution to the energy of aligned states.

C. Yrast bands

The comparison between the observed and CNSB rotational energies of ^{161}Lu as a function of spin is shown in Figs. 6 and 7, for the positive and negative parity bands, respectively. The reference energies of a rotating liquid drop are subtracted. The macroscopic energy used here is fitted with the pairing treated with the BCS approach [22], while particle-number projection is carried out in the present calculation. It was noticed that the particle-number projection procedure not only has effects on the pairing gap but also on the pairing correction energy and thus on the nuclear mass which becomes lowered by 1–2 MeV for the ground states [25]. In some studies [5,6], the vacuum energy given by the number-projected approaches are lower than that with the BCS approach and more close to the exact solutions. The energy differences between the BCS and PNP approach for the $1/2^+$ ground state and the $9/2^-_1$ band head, respectively, in ^{161}Lu are 1.06 and 1.04 MeV, even with the additional factor 0.95 multiplied to the G parameter in the PNP approach. Thus we have shifted the calculated results with the PNP approach upward 1.06 MeV in the paired results in Figs. 6 and 7. With this amendment, typical errors between the calculated and experimental results of yrast bands are in the range of ± 0.5 MeV with the CNSB model. However, it would be more proper to refit the macroscopic mass model with the pairing treated by the PNP approach in the future.

In Refs. [11,14], the configurations of yrast bands in ^{161}Lu were assigned and the features of the low-lying spectra

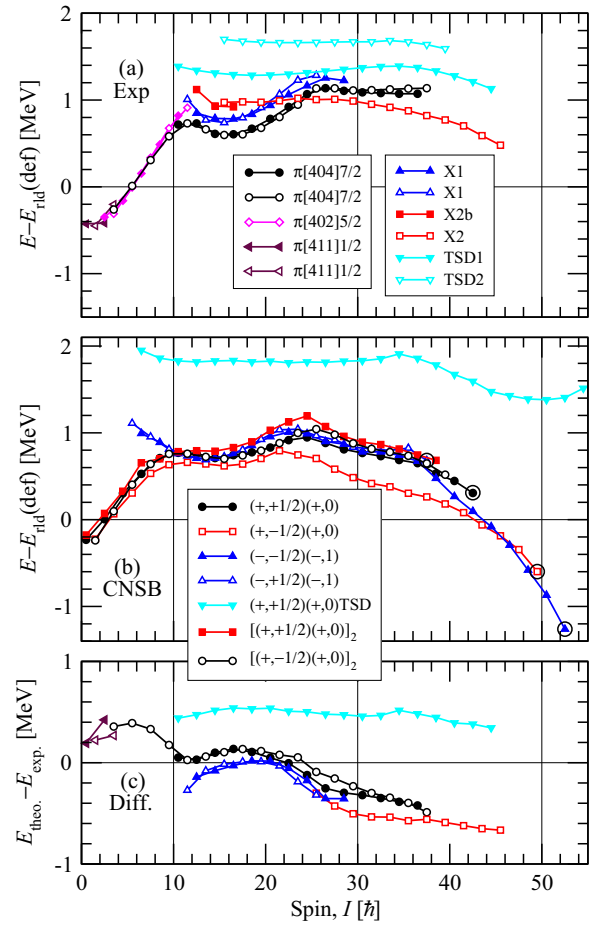

FIG. 6. (Color online) The experimental (a) and theoretical (b) energies and their differences (c) for the positive parity bands in ^{161}Lu. The subscript 2 indicates the theoretical yrare bands. Generally, the same symbols and line types are used in the three panels for the observed bands and the configurations assigned to them. However, the low spin states labeled as [411] 1/2 are compared with the (+, − 1/2)(+,0) and (+, − 1/2)(+,0) configurations, which are drawn by red squares because the high spin region of the (+, − 1/2)(+,0) configuration is assigned to the X2 band. Considering that no linking transition between the TSD1 and ND bands was observed, the energy of the lowest $21/2^+$ state of TSD1 was placed at 2.7 MeV so that this band is slightly higher in energy than the ND bands.

were discussed. Here, we will interpret these bands from comparisons with the CNSB calculations in Figs. 6 and 7, and compare with previous assignments.

1. Positive parity yrast bands

The deformation of the positive parity ground state is predicted to be close to prolate with $\varepsilon_2 \sim 0.18$. The proton [411]1/2, [402]5/2, and [404]7/2 orbitals are very close to each other and to the Fermi level around this deformation. Experimentally, all three bands based on these orbitals have been observed and are strongly mixed with each other with abundant interband transitions. Because of the large signature splitting of the [411]1/2 orbitals, the (+, − 1/2)(+,0) band with the CNSB model is built from the $\alpha = -1/2$ branch of

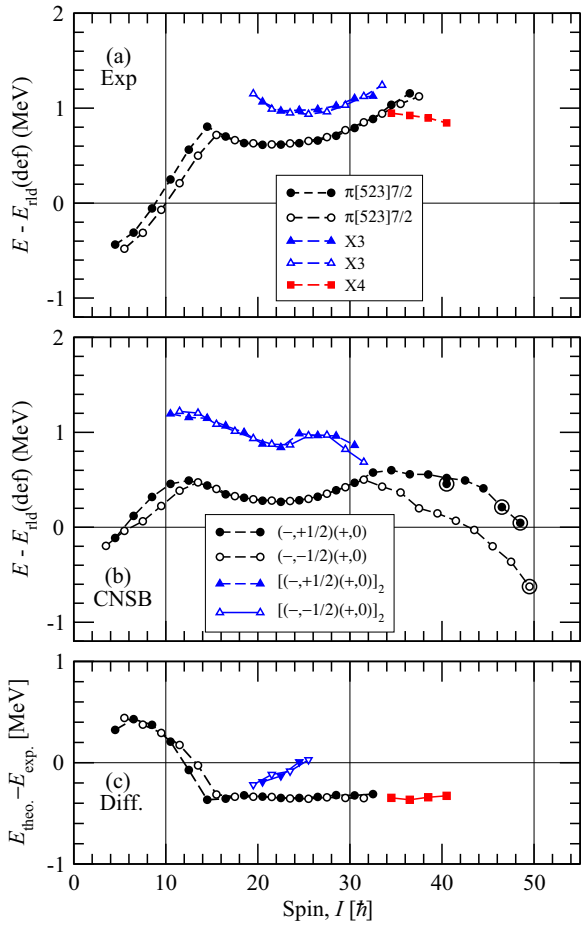

FIG. 7. (Color online) Same as previous figure but for the negative parity bands in ^{161}Lu. The configuration of the experimental yrast bands is assigned as $\pi[523]7/2$ which is different from the previous assignment $\pi[514]9/2$ in Ref. [14]; see text for details.

the [411]1/2 orbitals. In the present calculations, in addition to the yrast states, the yrare bands of the $(+,\pm 1/2)(+,0)$ configurations are also tentatively given in Fig. 6, where they are labeled with the subscript 2. The calculated signature splitting of the $(+,-1/2)(+,0)$ and $[(+,+1/2)(+,0)]_2$ bands is very small suggesting that they should be assigned to the experimental [404]7/2 bands.

For the positive parity yrast bands, the experimental first back-bending from the alignment of two $i_{13/2}$ quasineutrons is well reproduced by the paired calculation. At $I \approx 23.5$, the alignment of a pair of $h_{11/2}$ quasiprotons is predicted, leading to the second back-bending. The resulting $(+,-1/2)(+,0)$ yrast band, which is predicted to terminate at $I = 49.5$, is assigned to the observed X2 band. This interpretation will be supported by the unpaired calculations in Sec. III D 2, where the details of the X2 band will be discussed. The second backbending of the [404]7/2 bands is predicted to be at $I \approx 25.5$ which is $\sim 2\hbar$ delayed comparing with the $(+,-1/2)(+,0)$ yrast band. This is in agreement with the experimental observation. Note, however, that for spin values below the back-bending, the favored signature of the [411]1/2 band is predicted to come slightly below the [404]7/2 band but only the [404]7/2 band is observed.

2. Negative parity yrast bands

The observed negative parity yrast band was assigned to the $[514]9/2^-$ orbital in Ref. [14]. However, in the CNS or CNSB calculations, the $[523]7/2^-$ orbital is much closer to the Fermi level than $[514]9/2^-$. In ^{163}Lu [15] the yrast negative parity band has a similar decay pattern as in ^{161}Lu; for example, the $E2$ decays between $\alpha = -1/2$ states are much stronger than the decays between $\alpha = 1/2$ states in both cases. Contrary to ^{161}Lu, the negative parity band in ^{163}Lu is assigned to $[523]7/2^-$, where a weak populated state $7/2^-$ is observed [15]. In ^{165}Lu, although a tentative $7/2^-$ state is reported, the corresponding band is assigned to be based on the $[514]9/2^-$ orbital [26]. These observations in ^{161,163,165}Lu make us convinced that the negative parity yrast band in ^{161}Lu should be labeled as $[523]7/2^-$.

Before the back-bending, the observed yrast $\pi = -$ bands show some signature splitting. This is understood from the triaxial deformation which is induced by the quasineutron for the softly deformed nucleus; see the discussion in Ref. [11]. The mechanism is well explained in Refs. [27,28]. Indeed, a large negative γ deformation for the $(-,-1/2)(+,0)$ band is predicted before the back-bending; see the illustration of PESs from low spin to terminating spin in Fig. 8. This is contrary to the signature partner, which is calculated to be close to a prolate in this spin range. Note also that the large triaxial deformation is consistent with the observed $B(M1)/B(E2)$ values [11].

The yrast negative parity bands undergo the first back-bending at $I \approx 14.5$. After the back-bending, the alignment of two $i_{13/2}$ quasineutrons drives the nucleus to prolate shape and the signature partners have similar deformation—hence the signature splitting disappears. At $I \approx 35$, new crossings are predicted in the CNSB or CNS models. The crossing in the $\alpha = -1/2$ branch results in a band which shows a favored termination at $I = 49.5^-$ (see Sec. III B), but which is not observed, while the crossing in the $\alpha = 1/2$ branch results in the X4 band according to our interpretation. These crossings are easier to understand in the unpaired formalism and will be considered in more detail in Sec. III D 4.

3. Transitional quadrupole moments

The calculated transition quadrupole moments Q_t for the yrast bands are given in Fig. 9. To be consistent, the same radius and diffuseness parameters are taken as in the calculation of the rigid-body moment of inertias, i.e., $r_0 = 1.16$ fm and $a = 0.6$ fm. Note that with these parameters, the Q_t values are 6%–7% smaller than with the parameters as $r_0 = 1.2$ fm and $a = 0.0$ fm normally used in the CNS calculations [29]. This is understood from the fact that with present definitions [22,30], the quadrupole moments will be independent of the diffuseness depth. The calculated Q_t values with the CNSB model are $\sim 5.0e$ b at lower spins and generally decrease with increasing spin when the bands approach the terminating state. This is consistent with the experimental transition moment

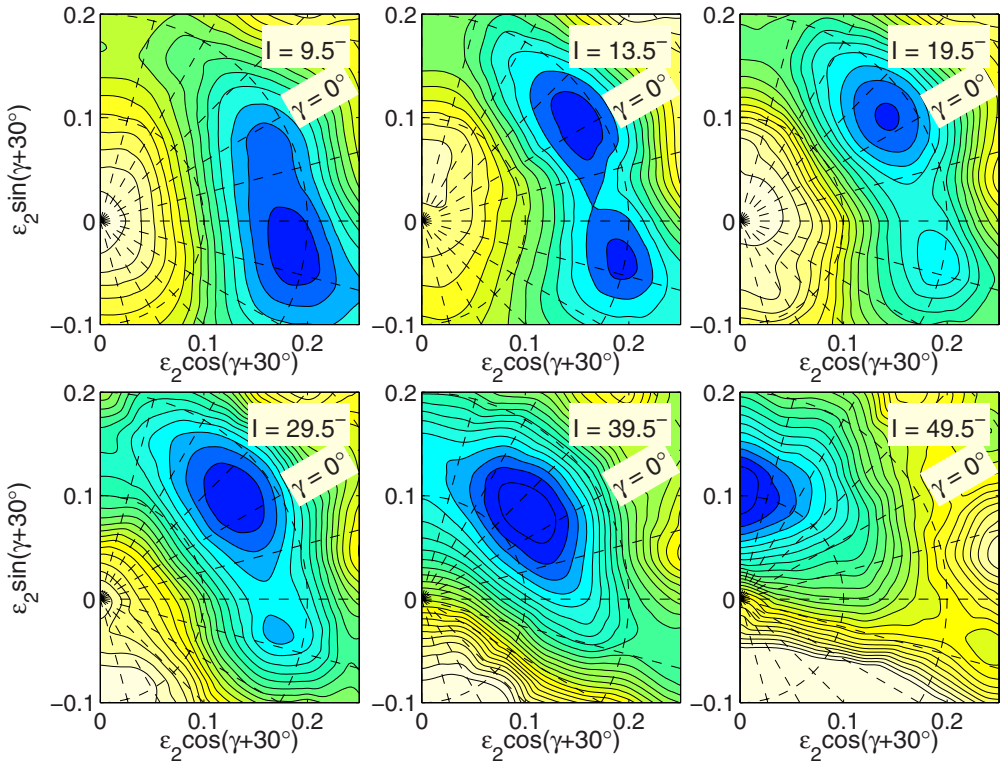

FIG. 8. (Color online) The PESs of the configuration $(-, -1/2)(+,0)$.

$Q_t = 5.2e$ b of the positive parity yrast bands at $I \approx 17.5$ [11].

D. Side bands

In the previous sections, the yrast bands in the low-spin and intermediate spin region were discussed. It was found that the experimental data were reproduced within $\sim \pm 0.5$ MeV by the CNSB model. Experimentally, several other bands have also been observed at higher spins (X2, X4) or higher excitation energies (X1, X3). In this section, these side bands will be discussed in detail. Particularly for the X2 band, the possibility of band termination is illustrated. At the small deformations calculated for the high spin bands in ^{161}Lu,

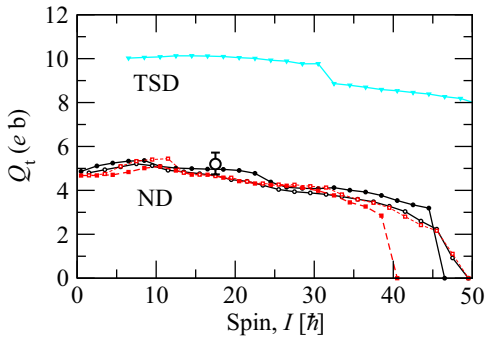

FIG. 9. (Color online) The transition quadrupole moments for the ND and TSD band in ^{161}Lu. The experimental value of the ND bands is taken from Ref. [11] and a 10% error is added.

the favored neutron configuration is $\nu(f_{7/2}h_{9/2})^6(i_{13/2})^2$ and this is the predicted configuration for the X2, X3, and X4 bands covered in this section. Consequently, these bands are distinguished by their proton configurations, which will be discussed below. Only the X1 band appears to have a negative parity neutron configuration.

1. X1 band

We start our discussion from the X1 band. For the positive parity, only one signature of the [404]7/2 band is observed below the paired crossing at $I \approx 12$ (see Fig. 6). Both signatures of the [402]5/2 band are seen below the crossing but there is no natural continuation after the crossing. Band X1 could be such a continuation which appears plausible from the observed energies, i.e., band X1 is about 0.2 MeV above the [404]7/2 band for spin values $I \approx 12$–25. However, band X1 mainly decays to the negative parity [523]7/2 band rather than to the [402]5/2 band. This suggests that it should have negative parity for protons and then negative parity also for the neutrons with a pair broken. Indeed, such bands are seen in Fig. 1 for the configurations which have negative parity for both protons and neutrons. One could also note that the positive and negative parity bands in ^{160}Yb which also differ by a broken neutron pair [31] have similar relative energies as the [523]7/2 and X1 bands in ^{161}Lu.

Four bands, two of each signature, match the above discussion. Only the $\alpha_n = 1$ bands, which are slightly lower in energy, are shown in Fig. 1. The question is then also which crossing is observed in the X1 band at similar spin/frequency as the yrast [404]7/2⊗ AB band. This crossing is seen both

in the experimental and theoretical results. According to the interpretation above, the X1 band has broken pairs for protons and neutrons, which makes the $h_{11/2}$ quasiproton or $[h_{9/2}f_{7/2}]$ quasineutron crossing less likely. We carried out fixed deformation calculations with different pairing gaps as well as unpaired calculations to answer this question. The back-bending appears in both paired and unpaired calculations around $I = 23.5$, which suggests that it is caused by an unpaired configuration change. Indeed, in the CNS calculations, a crossing is calculated between the $\nu[(h_{9/2}f_{7/2})^5(i_{13/2})^3]$ and $\nu[(h_{9/2}f_{7/2})^7(i_{13/2})^1]$ configurations for spin values just above $20\hbar$, where the $(i_{13/2})^3$ configuration is lower in energy at high spin from the high alignment of low-Ω $i_{13/2}$ orbitals.

2. X2 band

In the experimental paper [14], the X2 band with a high moment of inertia is tentatively interpreted as a TSD-like band at a triaxial shape, with a larger γ and smaller ε_2 than the other TSD bands. However, this band interacts with the ND bands, which puts such an interpretation in doubt. A band very similar to the X2 band is predicted by the CNSB model for spin values above $I = 20$, namely the $(+, +1/2)(+,0)$ configuration (see Fig. 6). Comparing with unpaired configurations at high spin in Fig. 1, except for a small difference in the slopes, this configuration and its signature partner are very similar in the CNS and CNSB configurations. We will therefore use the CNS formalism to discuss the configurations at high spin.

According to the interpretation in Sec. III C 1, the [404]7/2 band and the X2 band differ by the number of particles which have their main amplitudes in the pseudospin partner subshells [32–34] of the $\mathcal{N} = 4$ shell, i.e., in the $d_{5/2}$ and $g_{7/2}$ subshells (dg orbitals) and in the $d_{3/2}$ and $s_{1/2}$ subshells (sd orbitals), respectively. For $Z = 70$, the active dg Nilsson orbitals are [404]7/2 and [402]5/2 while [411]1/2 is the only active sd orbital (see Fig. 10). This figure is drawn at $\gamma = 10^\circ$, which means that the [402]5/2 and [404]7/2 orbitals are strongly mixed.

To describe the relation between the [404]7/2 and X2 bands (and also the crossings in connection with the X4 band; see below), it is thus necessary to be able to distinguish between dg orbitals and sd orbitals, This is contrary to standard CNS calculations, where all these orbitals are all labeled as low-j $\mathcal{N} = 4$. However, the distinction of dg and sd orbitals have been applied previously for some configurations which are close to termination, i.e., the deformation is close to the noncollective axis at $\gamma = 60^\circ$ [35,36]. The present bands in ^{161}Lu are further away from termination but even so, the calculated deformations are small and rather close to the $\gamma = 60^\circ$ axis. Indeed, in the limited region of the deformation space which is covered by the present bands, it turns out to be rather straightforward to distinguish between orbitals of dg and sd character, i.e., the $\mathcal{N} = 4$ orbitals which emerge from the pseudospin partner subshells below and above the spherical $Z = 64$ gap.

The observed [404]7/2 and X2 bands are shown relative to the rotating liquid drop model in the upper panel of Fig. 11 with the calculated bands assigned to them in the middle panel and the difference between calculations and experiment in the lower panel. The configurations assigned to the two observed bands are illustrated at $\hbar\omega \approx 0.2$ MeV in the single-particle diagram in Fig. 10; they have six occupied $h_{11/2}$ proton orbitals but differ by an $\mathcal{N} = 4$ proton. Thus, in the transition from the [404]7/2 to the X2 band, a proton is "deexcited" from the sd to the dg orbitals, i.e., from the [404]7/2 to the [411]1/2 Nilsson orbital. This means that the X2 band has all the dg orbitals occupied, i.e., a closed spherical $Z = 64$ core, corresponding to the configuration labeled [411]1/2 in Sec. III C 1. Furthermore, the configuration assigned to this band is built from one of the six favored terminations discussed in Sec. III B. It is built from the proton and neutron configurations terminating at $I_p = 19.5^+$ and $I_n = 30^+$, respectively, in Fig. 3, i.e., corresponding to the low-lying terminating $(+, +1/2)(+,0)$ band in Fig. 5. As seen in Figs. 1 and 2, of the six configurations which are predicted to terminate in the yrast region for $I = 49.5 - 52.5$, this one is calculated to be lowest in energy at intermediate spin values and should therefore be most easy to observe.

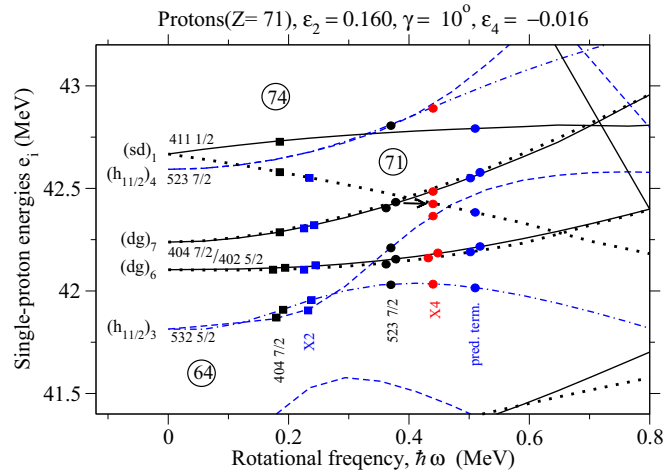

FIG. 10. (Color online) The single-proton Routhians drawn at a typical deformation of the high spin bands in ^{161}Lu. At $\omega = 0$, the orbitals are labeled according to their main amplitudes, dg ($d_{5/2}$ and $g_{7/2}$), sd ($d_{3/2}$ and $s_{1/2}$), and $h_{11/2}$, respectively, with the ordering within the groups as subscripts. Approximate asymptotic quantum numbers are also specified. The filling of the orbitals in the configurations associated with the X2 and X4 bands is illustrated. Furthermore, the configuration with five $h_{11/2}$ and two sd protons which is predicted to terminate in a low-energy state at $I = 49.5^-$ is illustrated at $\hbar\omega = 0.51$ MeV.

The X2 band is observed to $I = 45.5$, i.e., two transitions short of termination according to the present interpretation. The observed band shows some small irregularities in the aligned angular momenta [14]. These irregularities manifest the different nature of this band compared with the TSD bands, which have a high collectivity and are therefore expected to be more regular. With the present interpretation where the band has a small collectivity because it is formed at a small and varying deformation, some irregularities are expected in line with observations.

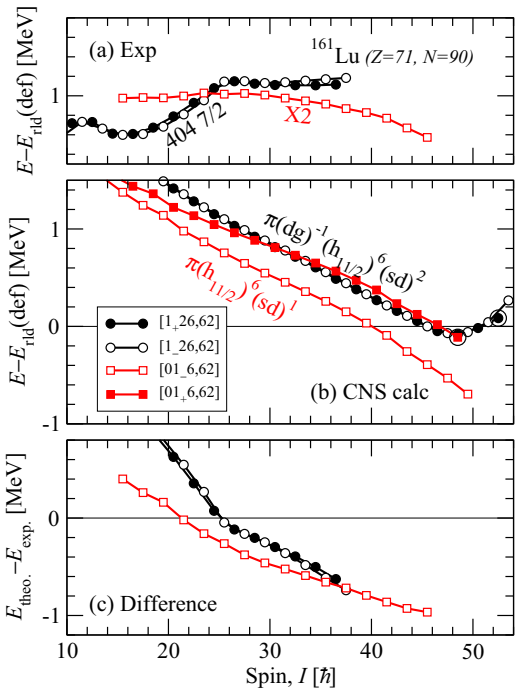

FIG. 11. (Color online) Comparison between the [404]7/2 and X2 bands and the CNS configurations assigned to them. In the middle panel, the filling of the proton orbitals is specified relative to a closed $Z = 64$ core, with the notation defined in the Fig. 10 caption. The detailed configurations relative to a $^{146}Gd_{82}$ core, $\pi(dg)^{-p_1}(sd)^{p_2}(h_{11/2})^{p_3}\nu(f_{7/2}h_{9/2})^{n_1}(i_{13/2})^{n_2}$, are given in the legend as $[p_1p_2p_3,n_1n_2]$. For an odd number of particles in a group, the subscript + or − defines the signature, $\alpha = 1/2$ or $\alpha = -1/2$.

Considering that pairing is neglected, the differences in Fig. 11(b) are in line with general expectations, i.e., the relative energies of the bands is essentially reproduced while the moment of inertia is off by 10% or so. Indeed, with pairing included, the calculated moments of inertia are close to experiment as seen from the fact that the differences in the lower panel of Fig. 6 are much more constant than those in Fig. 11. The observation that pairing must be included to reproduce the moments of inertia for $I \approx 30$ is in line with previous results for other nuclei in the $A \approx 155$–160 region. It can be seen, for example, from the comparison between calculations and experiment in ^{158}Er [24] and ^{156}Dy [37] or from the fact that different reference energies have been used for observed and calculated bands in ^{155}Dy [38] and ^{154}Dy [39].

As seen in Sec. III C 1, the configurations assigned to both the [404]7/2 and X2 bands are predicted to go through a paired $h_{11/2}$ quasiproton band crossing at spin values $I \approx 22$ while it is only in the [404]7/2 band that such a crossing is observed. The configuration of the X2 band is only observed when the $h_{11/2}$ protons are already aligned. However, the CNSB calculations predict that the [411]1/2 band, $(+, -1/2)(+,0)$, where the $h_{11/2}$ protons are paired off is competitive with the [404]7/2 band for spin values below $I \approx 22$. No such structure was observed but it should be a challenge for future experiments to find it.

Band X2b might be assigned as the yrare $(+1/2)(+,0)_2$ band, but because it is observed in such a short spin range, any assignment is very tentative.

3. X3 band

The large number of links between the yrast negative parity band and the X3 band indicates that both these bands have a common origin, i.e., they are both based on $h_{11/2}$ orbitals as previously concluded in Ref. [14]. However, in that reference, the X3 band was assigned to the [523]7/2 orbital, while we have argued in Sec. III C that it is instead the yrast band which is built from this orbital. In turn, this suggests that the X3 band is built from lifting the odd proton to the next $h_{11/2}$ orbital, [514]9/2, or making a hole in the next lower $h_{11/2}$ orbital, [532]5/2. Then, in the single-particle diagram, the energies of the [514]9/2 orbitals are too far away from the Fermi surface, which leaves [532]5/2 as the only reasonable interpretation of the X3 band.

The [532]5/2 should then correspond to the yrare $(-, \pm 1/2)(+,0)$ band. This configuration is tentatively calculated in the CNSB model and drawn in the spin range $10.5 \leq I \leq 31.5$ in Fig. 7(b), where it is denoted as $(-, \pm 1/2)(+,0)_2$. Up to spin values $I \approx 26.5$,, the CNSB results agree fairly well with the experimental data. Then, however, the calculated band goes through a band crossing, leading to down-sloping configuration. One may note that in the calculated yrast band, the $(-, -1/2)(+,0)_2$ configuration goes through a similar band crossing at $I \approx 32$ while the observed band continues smoothly to higher spin values.

4. X4 band

The X4 band is observed in the spin range $I = 34.5 - 40.5$. From Fig. 7, it is seen that it is well described by the yrast $(-,1/2)(+,0)$ band, but it is not straightforward to determine its structure in the paired formalism. Comparing with the unpaired calculations in Fig. 2, it appears that the same crossings are observed which suggests that the configuration change in the "crossing" between the [523]7/2 band and the X4 band can be determined in an unpaired formalism.

The single-proton orbitals at the approximate deformation of the $(-,\pm)(+,0)$ configuration for $I = 30 - 35$ are drawn as functions of rotational frequency in Fig. 10. With negative parity for the protons, the optimal filling of the orbitals is shown for $\hbar\omega \approx 0.37$ MeV, where two signature degenerate bands are formed with the odd proton in one or the other signature of the [523]7/2 orbital, i.e., this is the approximate filling of the orbitals in the high spin range of the [523]7/2 band where the pairing correlations are weak. Going to higher frequencies, there is a crossing between the [404]7/2 orbitals and the $\alpha = -1/2$ signature branch of the [411]1/2 orbital. After this crossing, it is energetically cheaper to put one of the [404]7/2 particles into this lowest [411]1/2 orbital instead. The filling of the orbitals in the corresponding configuration, which is assigned to the X4 band, is illustrated at $\hbar\omega \approx 0.44$ MeV. In this case there is an odd proton in each of the two orbitals [523]7/2 and [404]7/2. Therefore, depending on the signature of these two particles, four bands are formed, two of each signature.

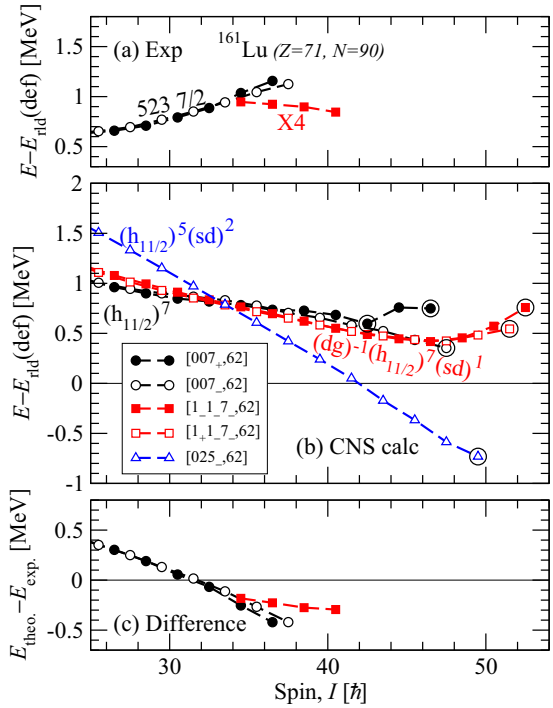

FIG. 12. (Color online) Same as Fig. 11, but for the X4 band and related configurations.

To describe the details of the configurations suggested for the [523]7/2 and X4 bands in Fig. 10, it is necessary to be able to distinguish between dg and sd orbitals, as discussed in connection with the X2 band above. With such a distinction, the calculated energies for the configurations illustrated in Fig. 10 are shown in the middle panel of Fig. 12. They are compared with the observed [523]7/2 and X4 bands in the upper panel with the difference between experiment and calculations in the lower panel.

As would be expected, the general features of the differences are similar in the lower panels of Figs. 11 and 12. Note, however, that the difference curve for the X4 band is rather flat, which means that for this configuration with one more pair broken, the moment of inertia is essentially reproduced also in the unpaired calculations. Note also that with the present interpretation, a signature degenerate partner to the X4 band is expected, but for such a weak band, it is not unexpected that only one signature branch is observed.

There is one more $(-,\pm)(+,0)$ band which comes low in energy for $I > 30$, namely the configuration with a closed $Z = 64$ core and with 5 $h_{11/2}$ and 2 sd valence protons, i.e., $\pi(h_{11/2})^5(sd)^2$ as illustrated at $\hbar\omega \approx 0.52$ MeV in Fig. 10. As seen in Fig. 12, it comes low in energy at high spin with a favored termination at $I = 49.5^-$. It is this configuration which explains the crossing within the $\alpha = -1/2$ orbitals in Fig. 2 at $I \approx 32$. However, this band has the wrong signature to be assigned to the observed X4 band. Because of the large signature splitting of the [523]5/2 orbital, the signature partner of the $(h_{11/2})^5(sd)^2$ band (not shown in Fig. 12) is calculated around 300 keV higher in energy and is therefore not a plausible interpretation of the X4 band. Note that with the present interpretation, none of the $(h_{11/2})^5(sd)^2$ bands are seen experimentally. This is not strange, however, because they correspond to a $2p2h$ excitation $[(h_{11/2})^{-2}(sd)^2]$ relative to the configuration assigned to the [523]7/2 band. This is contrary to the configuration assigned to the X4 band which is formed from a $1p1h$ configuration relative to the [523]7/2 band.

E. TSD bands

The TSD bands in Lu isotopes have been extensively studied in the last two decades [13,40–43]. In the neighboring Hf ($Z = 72$) isotopes, evidences for TSD bands have also been presented [44–47]. The cranking formalism has predicted pronounced minima around $(\varepsilon_2,\gamma) \sim (0.4,20^\circ)$ which are caused by shell gaps for proton numbers $Z = 71$ and 72, and neutron numbers $N = 94$ and 97 [40,48]. The observed markedly enhanced transition quadrupole moments of the TSD bands comparing with the ND bands in ^{163,164,165}Lu [49–52] shows that these bands have an enhanced deformation. Furthermore, the wobbling bands observed in ^{163,165,167}Lu and possibly ^{161}Lu can only be formed at triaxial deformation.

In the present CNSB model, $(+, +1/2)(+,0)$ is the lowest in energy configuration in the TSD minima of ^{161}Lu, $(\varepsilon_2,\gamma) \sim (0.40,20^\circ)$. This is true for spins up to $I \approx 50$, i.e., for all spin values where TSD bands have been observed in Lu isotopes. The rotational energies of this minimum are shown in Fig. 6 (cyan triangle-down). No linking transition between the TSD1 and ND bands was observed in ^{161}Lu. In the neighboring ^{163,165,167}Lu where the linking transitions have been observed, the TSD1 bands are generally a few hundred keV above the yrast bands. Therefore the band head of TSD1 in ^{161}Lu is placed at an arbitrary energy, 2.7 MeV, to keep the systematics. From Fig. 6 it is interesting to see that the moment of inertia is similar for the theoretical results and the experimental observations so that the energy differences between them remain flat for the entire spin range. This is a clear improvement compared with the CNS calculations [53], where the missing pairing energy leads to a difference curve with a pronounced curvature, which slopes downwards with increasing spin. The change of slope at spin $I = 36.5$ is well reproduced by the CNSB calculations. In the CNS analyses, the configuration with four neutrons in the $i_{13/2}$ orbitals becomes lower in energy for $I \geqslant 36.5$ than the configuration with six neutrons in $i_{13/2}$ [53], i.e., the configuration where also the Nilsson orbitals are occupied which would be labeled [642] 5/2 at axial shape. From the PESs in Fig. 13, we can see that two triaxial shapes coexist at $I^\pi = 34.5^+$ around $(0.4,20^\circ)$, with the quadrupole deformation of one minimum slightly smaller than the other. For $I \leqslant 34.5$ the minimum lies at larger $\varepsilon_2 \approx 0.42$ and the minimum shifts to the smaller $\varepsilon_2 \approx 0.37$ region for $I \geqslant 36.5$. By occupying the [400]1/2 orbitals instead of the $i_{13/2}$, [642]5/2 orbitals, the ^{161}Lu nucleus becomes less deformed at higher spins. The shift of the deformation will have an effect on the transition moments of this TSD band. Thus, as shown in Fig. 9, a small decrease in Q_t values is calculated because of the shape change. For the TSD bands of other Lu isotopes with $N \geqslant 92$, all the [400]1/2 and [642]5/2 orbitals are occupied, therefore the drop of Q_t values is unique for ^{161}Lu.

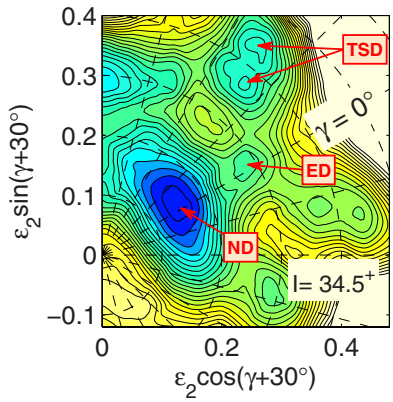

FIG. 13. (Color online) The PES of the $(+,+1/2)(+,0)$ configuration at $I = 34.5$ in ^{161}Lu. The ND, ED, and TSD indicate the normal deformed, enhanced deformed, and triaxial strongly deformed shapes.

IV. SUMMARY AND CONCLUSIONS

The paired cranked Nilsson-Strutinsky-Bogoliubov (CNSB) model is presented, which employs the same method to calculate the liquid-drop energy and moment of inertia as the unpaired cranked Nilsson-Strutinsky (CNS) model. In the CNSB model, the energy minimization is carried out in a mesh of pairing gaps and Fermi levels as well as deformation parameters. As exemplified in Figs. 4, 8, and 13, it becomes possible to draw smooth energy surfaces in the full (ε_2,γ) plane in this formalism.

Based on a comparative study using the CNSB and CNS models, it is concluded that ^{161}Lu is a favorable case for formation of bands which terminate as yrast at the maximal spin value in valence space, $I \approx 50$. In general, the relative energy of aligned and nonaligned states in the terminating region is similar with and without pairing. However in specific cases where the quasiparticle orbitals near the Fermi surface are not blocked, pairing can be important giving a larger contribution to the energy of aligned states.

The complete high spin spectra including the normal deformed (ND) bands, the triaxial strongly deformed (TSD) bands, the observed side bands, and the terminating bands in ^{161}Lu are interpreted. The experimental rotational energies are reproduced within $\sim \pm 0.5$ MeV by the CNSB model. At spin values above the neutron $i_{13/2}$ and proton $h_{11/2}$ band crossings, the relative energies of the different bands are well described by the unpaired CNS calculations while the pairing gives small contributions to the moments of inertia. The [523]7/2 orbital is assigned to the negative parity yrast bands, contrary to the assignment in Ref. [14], [514]9/2. For the side bands, we argued that the X1 band is not a continuation of the π[402]5/2 band but is built from a negative parity proton and a broken neutron pair with one neutron in a negative parity orbital. The [532]5/2 configuration is tentatively assigned to the X3 band.

The transparent analyses on the rotational structure of the X2 and X4 bands becomes possible from comparisons with the unpaired CNS model, where a distinction is made of the $\mathcal{N} = 4$ pseudospin partners of $(d_{5/2},g_{7/2})$ and $(d_{3/2},s_{1/2})$ character, respectively. The X2 band was originally assigned as a band of TSD nature but, from comparisons with calculated CNS energies it was argued in Ref. [16] that it should rather be understood as a terminating band observed two transitions short of the fully aligned state. This conclusion gets strong support from the detailed understanding of the configuration change when the X2 band feeds into the [404] 7/2 band. The configurations assigned to the X2 and X4 bands have in common that the highly favored $\alpha = -1/2$ branch of the [411]1/2 orbitals is occupied, which gives a comparatively large angular momentum contribution leading to a favored energy at high spin.

With the pairing correlation included, the experimental rotational energies of the TSD1 band in ^{161}Lu are well reproduced in the CNSB model. The observed energies indicate a band crossing at $I \approx 36$. It is correlated with a calculated configuration change leading to a shift of deformation from $(\varepsilon_2,\gamma) \sim (0.42,20^\circ)$ for $I \leqslant 34.5$ to $\sim (0.37,20^\circ)$ for $I \geqslant 36.5$. The shape shift will result in a drop of transition quadrupole moments at high spins, which is unique among the TSD bands of the ^{161,163,165,167}Lu isotopes.

ACKNOWLEDGMENTS

This project is supported by the Swedish Science Research Council. One of our authors, Hai-Liang Ma wants to acknowledge support from the NSF of China under Contracts No. 11205245 and No. 11375266 and the support of a guest scholarship from the Swedish Institute.

[1] S. Pancholi, *Exotic Nuclear Excitations*, Springer Tracts in Modern Physics (Springer, New York, 2011).
[2] M. J. A. de Voigt, J. Dudek, and Z. Szymański, Rev. Mod. Phys. **55**, 949 (1983).
[3] Y. R. Shimizu, J. D. Garrett, R. A. Broglia, M. Gallardo, and E. Vigezzi, Rev. Mod. Phys. **61**, 131 (1989).
[4] P. Ring and P. Schuck, *The Nuclear Many-Body Problem* (Springer, New York, 2000).
[5] W. Nazarewicz, J. Dudek, and Z. Szymański, Nucl. Phys. A **436**, 139 (1985).
[6] J. A. Sheikh, P. Ring, E. Lopes, and R. Rossignoli, Phys. Rev. C **66**, 044318 (2002).
[7] B. G. Carlsson, I. Ragnarsson, R. Bengtsson, E. O. Lieder, R. M. Lieder, and A. A. Pasternak, Phys. Rev. C **78**, 034316 (2008).
[8] M. Anguiano, J. Egido, and L. Robledo, Nucl. Phys. A **696**, 467 (2001).
[9] J. A. Sheikh and P. Ring, Nucl. Phys. A **665**, 71 (2000).
[10] A. V. Afanasjev, D. B. Fossan, G. J. Lane, and I. Ragnarsson, Physics Reports **322**, 1 (1999).
[11] C. H. Yu *et al.*, Nucl. Phys. A **489**, 477 (1988).
[12] P. Bringel *et al.*, European Physical Journal A **16**, 155 (2003).

[13] P. Bringel *et al.*, The European Physical Journal A—Hadrons and Nuclei **24**, 167 (2005).
[14] P. Bringel *et al.*, Phys. Rev. C **73**, 054314 (2006).
[15] D. Jensen *et al.*, The European Physical Journal A—Hadrons and Nuclei **19**, 173 (2004).
[16] I. Ragnarsson, B. G. Carlsson, and H. Ryde, Int. J. Mod. Phys. E **19**, 590 (2010).
[17] J. C. Marsh *et al.*, Phys. Rev. C **88**, 041306 (2013).
[18] T. Bengtsson, Nucl. Phys. A **496**, 56 (1989).
[19] S. G. Nilsson and I. Ragnarsson, *Shapes and Shells in Nuclear Structure* (Cambridge University Press, Cambridge, 1995).
[20] V. Strutinsky, Nucl. Phys. A **95**, 420 (1967).
[21] K. Pomorski and J. Dudek, Phys. Rev. C **67**, 044316 (2003).
[22] B. G. Carlsson and I. Ragnarsson, Phys. Rev. C **74**, 011302 (2006).
[23] T. Bengtsson, Nucl. Phys. A **512**, 124 (1990).
[24] J. Simpson *et al.*, Phys. Lett. B **327**, 187 (1994).
[25] H. Olofsson, R. Bengtsson, and P. Möller, Nucl. Phys. A **784**, 104 (2007).
[26] G. Schönwaßer *et al.*, Nucl. Phys. A **735**, 393 (2004).
[27] S. Frauendorf and F. May, Phys. Lett. B **125**, 245 (1983).
[28] Y. S. Chen, S. Frauendorf, and G. A. Leander, Phys. Rev. C **28**, 2437 (1983).
[29] X. Wang, Phys. Lett. B **702**, 127 (2011).
[30] K. T. R. Davies and J. R. Nix, Phys. Rev. C **14**, 1977 (1976).
[31] L. L. Riedinger, Physica Scripta **1983**, 36 (1983).
[32] A. Arima, M. Harvey, and K. Shimizu, Phys. Lett. B **30**, 517 (1969).
[33] R. D. Ratna Raju, J. P. Drayer, and K. T. Hecht, Nucl. Phys. A **202**, 433 (1973).
[34] A. Bohr, I. Hamamoto, and B. R. Mottelson, Physica Scripta **26**, 267 (1982).
[35] A. O. Evans *et al.*, Phys. Rev. Lett. **92**, 252502 (2004).
[36] Purnima Singh *et al.*, Phys. Rev. C **85**, 034319 (2012).
[37] F. G. Kondev *et al.*, Phys. Lett. B **437**, 35 (1998).
[38] I. Ragnarsson, Acta Phys. Pol. B **27**, 33 (1996).
[39] W. C. Ma *et al.*, Phys. Rev. C **65**, 034312 (2002).
[40] H. Schnack-Petersen *et al.*, Nucl. Phys. A **594**, 175 (1995).
[41] S. W. Ødegård *et al.*, Phys. Rev. Lett. **86**, 5866 (2001).
[42] G. Schönwaßer *et al.*, Phys. Lett. B **552**, 9 (2003).
[43] H. Amro *et al.*, Phys. Lett. B **553**, 197 (2003).
[44] A. Neußer-Neffgen *et al.*, Phys. Rev. C **73**, 034309 (2006).
[45] S. Mukhopadhyay *et al.*, Phys. Rev. C **83**, 044311 (2011).
[46] D. Hartley *et al.*, Phys. Lett. B **608**, 31 (2005).
[47] D. T. Scholes *et al.*, Phys. Rev. C **70**, 054314 (2004).
[48] R. Bengtsson and H. Ryde, The European Physical Journal A—Hadrons and Nuclei **22**, 355 (2004).
[49] W. Schmitz *et al.*, Phys. Lett. B **303**, 230 (1993).
[50] G. Schönwaßer *et al.*, The European Physical Journal A—Hadrons and Nuclei **13**, 291 (2002).
[51] A. Görgen *et al.*, Phys. Rev. C **69**, 031301 (2004).
[52] G. Gürdal *et al.*, Journal of Physics G: Nuclear and Particle Physics **31**, S1873 (2005).
[53] A. Kardan, I. Ragnarsson, H. Miri-Hakimabad, and L. Rafat-Motevali, Phys. Rev. C **86**, 014309 (2012).